

Transmission and Goos-Hänchen like Shifts through a Graphene Double Barrier in an Inhomogeneous Magnetic Field

Miloud Mekkaoui^a, Ahmed Jellal^{*a,b} and Hocine Bahloul^{b,c}

^a*Theoretical Physics Group, Faculty of Sciences, Chouaïb Doukkali University,
PO Box 20, 24000 El Jadida, Morocco*

^b*Saudi Center for Theoretical Physics, Dhahran, Saudi Arabia*

^c*Physics Department, King Fahd University of Petroleum & Minerals,
Dhahran 31261, Saudi Arabia*

Abstract

We studied the transport properties of electrons in graphene as they are scattered by a double barrier potential in the presence of an inhomogeneous magnetic field. We computed the transmission coefficient and Goos-Hänchen like shifts for our system and noticed that transmission is not allowed for certain range of energies. In particular, we found that, in contrast to the electrostatic barriers, the magnetic barriers are able to confine Dirac fermions. We also established some correlation between the electronic transmission properties of Dirac fermions with the Goos-Hänchen like shifts, as reflected in the numerical data.

PACS numbers: 73.63.-b; 73.23.-b; 72.80.Rj

Keywords: graphene, double barrier potential, Dirac equation, transmission, Goos-Hänchen like shifts.

*ajellal@ictp.it – a.jellal@ucd.ac.ma

1 Introduction

Graphene, a planar arrangement of carbon atoms on a honeycomb lattice, is a unique realization of a two dimensional electronic system. Due to its excellent carrier transport properties, graphene has a great potential for nano-electronic applications. Among the peculiar electronic properties of this 2D-material is its unusual quantum Hall effect [1]. Graphene is also a transparent conductor [2] whose carriers are massless and chiral relativistic fermions governed by a Dirac-like equation leading to many fascinating physical properties of graphene, such as Klein tunneling [3,4]. However, as appealing as the Klein tunneling may sound from the fundamental research point of view, its presence in graphene is unwanted when it comes to applications of graphene because space confinements of the carriers is of great importance in nanoelectronic applications. In addition, the ability to control electronic properties of a material by an externally applied voltage is at the heart of modern electronics [5,6].

The inability to confine electrons using an electrostatic potential barrier severely limited the applicability of graphene based devices. However, it came as a big relief when it was pointed out that well localized magnetic field dubbed as magnetic barrier can confine massless Dirac fermions in graphene [7]. Later on, snake states, trajectories of charge carriers curving back and forth along interfaces, were proven to play an important role and were studied experimentally [8,9], mainly motivated by the quest for electrical rectification. The inhomogeneous magnetic field case in graphene was analyzed in [7]. Theoretically, electron waveguides, in graphene subject to a suitable inhomogeneous magnetic field, were considered in [10]. One of the interesting features of such inhomogeneous magnetic field profile is that it can bind electrons, contrary to the usual potential step. Such a step magnetic field will indeed result in electron states that are bound to the B_j -field step and are able to move only in one direction, along the step.

During the past few years there was substantial progress in studying electron transport properties in graphene, among these developments we cite the quantum version of the Goos-Hänchen effect originating from the reflection of particles from interfaces. Many works on various graphene-based nanostructures, including single barrier [11], double barrier [12,13] and superlattices [15], showed that the Goos-Hänchen like (GHL) shifts can be enhanced by the transmission resonances and controlled by varying the electrostatic potential and induced gap [11]. Similar to the situation in semiconductors, the GHL shifts in graphene can also be modulated by electric and magnetic barriers [16], and atomic optics [17]. It has been reported that the GHL shifts have a major effect on the group velocity of quasiparticles along interfaces of graphene p-n junctions [18,19].

Very recently, the GHL shifts for Dirac fermions in graphene scattered by double barrier structures have been studied in [13]. Moreover, in [14] we have explored the zero, positive and negative quantum GHL shifts of the transmitted Dirac carriers in graphene through a potential barrier with vertical magnetic field. Numerical results show that only one energy position at the zero GHL shift exists and is highly dependent on the y -directional wave vector, the energy gap, the magnetic field and the potential. The positive and negative GHL shifts happen when the incident energy is more and less than the energy position at the zero GHL shift, respectively. In addition, we found that there are two values of potential at the zero GHL shifts, where a potential window can always keep the positive GHL shifts. These results may be useful in designing a graphene-based valley or spin splitter as well as manipulating the electrons and holes in graphene nanostructure.

Motivated by different developments on the subject and in particular as a follow up on our recent works [13, 14], we investigate the GHL shifts in a gaped graphene system in the presence of an inhomogeneous magnetic field and a double barrier potential. We separate our system into three regions and determine the solutions of the energy spectrum in each region. Matching the wave functions at both interfaces, we then calculate the transmission coefficient as well as the GHL shifts. To allow a better understanding of our results, we study the transmission coefficient as well as the GHL shifts while varying different physical parameters that characterize our system.

This paper is organized as follows. In section 2, we formulate our system Hamiltonian describing particles scattered in graphene by a double barrier potential in the presence of an inhomogeneous magnetic field. We then obtain the solutions of the energy spectrum corresponding to each region in terms of different physical parameters and analyze the energy conservation law. In section 3, the scattering problem for Dirac fermions will be solved using continuity at the boundary, which will enable us to calculate the transmission coefficient and corresponding phase. The condition for full reflection are then obtained for certain incidence angles ϕ_1 . In section 4, we study the GHL shifts and transmission coefficient as well as discuss our main results. We present our main conclusions in the final section.

2 Theoretical model

We consider a system of massless Dirac fermions moving through a strip of graphene and subject to a potential, which has the form shown in the Figure 1. The system contains five regions denoted by the index $j = 1, 2 \dots, 5$. The left region ($j = 1$) describes the incident electron beam with energy $E = v_F \epsilon$ and incident angle ϕ_1 where v_F is the Fermi velocity. The far right region ($j = 5$) describes the transmitted electron beam with a lateral shift S_t and angle ϕ_5 but in the presence of an inhomogeneous magnetic field. We introduce in the intermediate regions $j = 2, 4$ and middle region $j = 3$ two different magnetic fields B_2 and B_3 , respectively, such as

$$B_j(x) = \begin{cases} B_2, & d_1 < |x| < d_2 \\ B_3, & |x| < d_1 \\ 0, & \text{otherwise.} \end{cases} \quad (1)$$

In the present study, we consider the system in an inhomogeneous magnetic field given by the configuration (1) in addition to the presence of an energy gap t'_j in the regions 2, 3 and 4 defined by

$$t'_j = \begin{cases} t'_2, & d_1 < |x| < d_2 \\ t'_3, & |x| < d_1 \\ 0, & \text{otherwise.} \end{cases} \quad (2)$$

In order to study the scattering of Dirac fermions in graphene by the above double barrier structure we first choose the following potential configuration

$$V_j(x) = \begin{cases} V_2, & d_1 < |x| < d_2 \\ V_3, & |x| < d_1 \\ 0, & \text{otherwise} \end{cases} \quad (3)$$

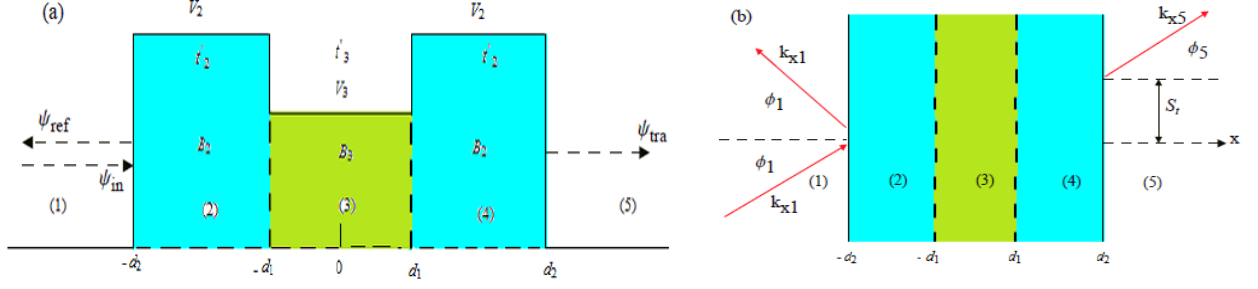


Figure 1: Schematic diagram for Dirac fermions in an inhomogeneous magnetic field and passing through a graphene double barrier, with height V_2 in the region $d_1 < |x| < d_2$ and height V_3 in the region $|x| < d_1$. (a) the dashed lines show smooth electric potentials having error function distributions. (b) describes the incident, reflected, and transmitted electron beams with a lateral shift S_t .

where j labels the five regions indicated schematically in Figure 1 that shows the space configuration of the potential profile. The Hamiltonian for one-pseudospin component in the j -th region can be written as

$$H_j = v_F \boldsymbol{\sigma} \cdot \boldsymbol{\pi} + V_j(x) \mathbb{I}_2 + t_j \sigma_z \Theta(d_2^2 - x^2) \quad (4)$$

where Θ is the Heaviside step function, $\boldsymbol{\pi} = p + eA_j/c$ is the two-component kinetic momentum with the canonical momentum $p = -i\hbar(\partial_x, \partial_y)^T$, $\boldsymbol{\sigma} = (\sigma_x, \sigma_y)$ and σ_z are the usual Pauli matrices, \mathbb{I}_2 is the 2×2 unit matrix. Choosing the Landau gauge we select the vector potential $\mathbf{A} = (0, Ay, 0)^T$ that creates the inhomogeneous magnetic field defined by (1), imposing the continuity of this vector potential at the boundaries of each region requires that

$$A_y(x) = A_j = \frac{c}{e} \times \begin{cases} \frac{1}{l_{B_2}^2}(d_1 - d_2) - \frac{1}{l_{B_3}^2}d_1, & x < -d_2 \\ \frac{1}{l_{B_2}^2}x + \left(\frac{1}{l_{B_2}^2} - \frac{1}{l_{B_3}^2}\right)d_1, & -d_2 \leq x \leq -d_1 \\ \frac{1}{l_{B_3}^2}x, & |x| < d_1 \\ \frac{1}{l_{B_2}^2}x - \left(\frac{1}{l_{B_2}^2} - \frac{1}{l_{B_3}^2}\right)d_1, & d_1 \leq x \leq d_2 \\ \frac{1}{l_{B_2}^2}(d_2 - d_1) + \frac{1}{l_{B_3}^2}d_1, & x \geq d_2 \end{cases} \quad (5)$$

where the local magnetic length is defined by $l_{B_j} = \sqrt{c/eB_j}$ in our selected system of units ($\hbar = 1$).

The eigenvalues and eigenspinors of H_j in regions 1 and 5 are generated by the Dirac Hamiltonian

$$H_j = \begin{pmatrix} 0 & v_F [p_{xj} - i(p_y + \frac{e}{c}A_j)] \\ v_F [p_{xj} + i(p_y + \frac{e}{c}A_j)] & 0 \end{pmatrix} \quad (6)$$

and the time independent Dirac equation for the spinor $\psi_j(x, y) = (\varphi_j^+, \varphi_j^-)^T$ associated with energy $E = v_F \epsilon$ is given by

$$H_j \begin{pmatrix} \varphi_j^+ \\ \varphi_j^- \end{pmatrix} = \epsilon \begin{pmatrix} \varphi_j^+ \\ \varphi_j^- \end{pmatrix} \quad (7)$$

which can be written as two linear differential equations of the form

$$\left[p_{xj} - i \left(p_y + \frac{e}{c} A_j \right) \right] \varphi_j^- = \epsilon \varphi_j^+ \quad (8)$$

$$\left[p_{xj} + i \left(p_y + \frac{e}{c} A_j \right) \right] \varphi_j^+ = \epsilon \varphi_j^- \quad (9)$$

The corresponding energy eigenvalues read as

$$\epsilon = s_j \sqrt{p_{xj}^2 + \left(p_y + \frac{e}{c} A_j\right)^2} \quad (10)$$

where the symbol $s_j = \text{sign}(\epsilon)$ and

$$p_{xj} = \sqrt{\epsilon^2 - \left(p_y + \frac{e}{c} A_j\right)^2}. \quad (11)$$

with incoming momentum $\mathbf{p}_j = (p_{xj}, p_y)$ and position $\mathbf{r} = (x, y)$. The incoming wave function takes the form

$$\psi_{in} = \frac{1}{\sqrt{2}} \begin{pmatrix} 1 \\ z_{p_{xj}} \end{pmatrix} e^{i\mathbf{p}_j \cdot \mathbf{r}} \quad (12)$$

and $z_{p_{xj}}$ is given by

$$z_{p_{xj}} = z_j = s_j \frac{p_{xj} + i(p_y + \frac{e}{c} A_j)}{\sqrt{(p_{xj})^2 + (p_y + \frac{e}{c} A_j)^2}} = s_j e^{i\phi_j} \quad (13)$$

where $s_0 = \text{sgn}(\epsilon)$ and $\phi_j = \arctan\left(\frac{p_y - \frac{e}{c} A_j}{p_{xj}}\right)$ is the angle that the incident electrons make with the x -direction, p_{x1} and p_y are the x and y -components of the electron wave vector, respectively. The eigenspinors read as

$$\psi_j^+ = \frac{1}{\sqrt{2}} \begin{pmatrix} 1 \\ z_j \end{pmatrix} e^{i(p_{xj}x + p_y y)} \quad (14)$$

$$\psi_j^- = \frac{1}{\sqrt{2}} \begin{pmatrix} 1 \\ -z_j^* \end{pmatrix} e^{i(-p_{xj}x + p_y y)}. \quad (15)$$

To be much more accurate, we give the solutions of the energy spectrum for each region. Then in region 1 ($x < -d_2$), we have

$$\epsilon = \sqrt{p_{x1}^2 + \left[p_y + \frac{1}{l_{B_2}^2}(d_1 - d_2) - \frac{1}{l_{B_3}^2}d_1\right]^2} \quad (16)$$

$$\psi_1 = \frac{1}{\sqrt{2}} \begin{pmatrix} 1 \\ z_1 \end{pmatrix} e^{i(p_{x1}x + p_y y)} + r \frac{1}{\sqrt{2}} \begin{pmatrix} 1 \\ -z_1^* \end{pmatrix} e^{i(-p_{x1}x + p_y y)} \quad (17)$$

$$z_1 = s_1 \frac{p_{x1} + i \left[p_y + \frac{1}{l_{B_2}^2}(d_1 - d_2) - \frac{1}{l_{B_3}^2}d_1\right]}{\sqrt{p_{x1}^2 + \left[p_y + \frac{1}{l_{B_2}^2}(d_1 - d_2) - \frac{1}{l_{B_3}^2}d_1\right]^2}} \quad (18)$$

and in region 5 ($x > d_2$), the solution is

$$\epsilon = \sqrt{p_{x5}^2 + \left[p_y + \frac{1}{l_{B_2}^2}(d_2 - d_1) + \frac{1}{l_{B_3}^2}d_1\right]^2} \quad (19)$$

$$\Psi_5 = \frac{1}{\sqrt{2}} t \begin{pmatrix} 1 \\ z_5 \end{pmatrix} e^{i(p_{x5}x + p_y y)} \quad (20)$$

$$z_5 = s_5 \frac{p_{x5} + i \left[p_y + \frac{1}{l_{B_2}^2}(d_2 - d_1) + \frac{1}{l_{B_3}^2}d_1\right]}{\sqrt{p_{x1}^2 + \left[p_y + \frac{1}{l_{B_2}^2}(d_2 - d_1) + \frac{1}{l_{B_3}^2}d_1\right]^2}}. \quad (21)$$

For the system under consideration, we can write the Hamiltonian corresponding to regions (2), (3) and (4) in matrix form as

$$H_j = v_F \begin{pmatrix} \frac{V_j}{v_F} + \frac{t'_j}{v_F} & -i \frac{\sqrt{2}}{l_{B_j}} \left[\frac{l_{B_j}}{\sqrt{2}} (\partial_{x_j} - i\partial_y + \frac{e}{c} A_j) \right] \\ i \frac{\sqrt{2}}{l_{B_j}} \left[\frac{l_{B_j}}{\sqrt{2}} (-\partial_{x_j} - i\partial_y + \frac{e}{c} A_j) \right] & \frac{V_j}{v_F} - \frac{t'_j}{v_F} \end{pmatrix}. \quad (22)$$

Note that the energy gap t'_j is equivalent to a mass term, this will lead to interesting consequences on the physical properties of such system. We determine the eigenvalues and eigenspinors of the corresponding Hamiltonian H by solving the time independent equation for the spinor $\psi_j(x, y) = (\psi_j^+, \psi_j^-)^T$. Since the transverse momentum p_y is conserved, we can then write the wave function as $\psi_j(x, y) = e^{ip_y y} \varphi_j(x)$, with $\varphi_j(x) = (\varphi_j^+, \varphi_j^-)^T$, and energy $E = v_F \epsilon$, which lead to

$$H_j \begin{pmatrix} \varphi_j^+ \\ \varphi_j^- \end{pmatrix} = \epsilon \begin{pmatrix} \varphi_j^+ \\ \varphi_j^- \end{pmatrix}. \quad (23)$$

At this stage, it is convenient to introduce the concepts of annihilation and creation operators in order to ease the diagonalization of our Hamiltonian. They can be defined by

$$a_j = \frac{l_{B_j}}{\sqrt{2}} \left(\partial_{x_j} + k_y + \frac{e}{c} A_j \right), \quad a_j^\dagger = \frac{l_{B_j}}{\sqrt{2}} \left(-\partial_{x_j} + k_y + \frac{e}{c} A_j \right) \quad (24)$$

and obey the canonical commutation relations $[a_j, a_k^\dagger] = \delta_{j,k}$. Rescaling our energies $t'_j = v_F \mu_j$ and $V_j = v_F v_j$, then (23) can be written in terms of a_j and a_j^\dagger as

$$\begin{pmatrix} v_j + \mu_j & -i \frac{\sqrt{2}}{l_{B_j}} a_j \\ +i \frac{\sqrt{2}}{l_{B_j}} a_j^\dagger & v_j - \mu_j \end{pmatrix} \begin{pmatrix} \varphi_j^+ \\ \varphi_j^- \end{pmatrix} = \epsilon \begin{pmatrix} \varphi_j^+ \\ \varphi_j^- \end{pmatrix} \quad (25)$$

giving rise to the two relations between spinor components

$$(v_j + \mu_j) \varphi_j^+ - i \frac{\sqrt{2}}{l_{B_j}} a_j \varphi_j^- = \epsilon \varphi_j^+ \quad (26)$$

$$i \frac{\sqrt{2}}{l_{B_j}} a_j^\dagger \varphi_j^+ + (v_j - \mu_j) \varphi_j^- = \epsilon \varphi_j^-. \quad (27)$$

Injecting (27) in (26), we obtain a second order differential equation for φ_j^+

$$\left[(\epsilon - v_j)^2 - \mu_j^2 \right] \varphi_j^+ = \frac{2}{l_{B_j}^2} a_j a_j^\dagger \varphi_j^+ \quad (28)$$

which shows clearly that φ_j^+ is an eigenstate of the number operator $\widehat{N}_j = a_j^\dagger a_j$ and therefore we identify φ_j^+ to be eigenstates of the harmonic oscillator $|n_j - 1\rangle$, namely

$$\varphi_j^+ \sim |n_j - 1\rangle \quad (29)$$

which is equivalent to stating

$$\left[(\epsilon - v_j)^2 - \mu_j^2 \right] |n_j - 1\rangle = \frac{2}{l_{B_j}^2} n_j |n_j - 1\rangle \quad (30)$$

and the energy spectrum can be defined by

$$\epsilon - v_j = s_j \epsilon_{n_j} = s_j \frac{1}{l_{B_j}} \sqrt{(\mu_j l_{B_j})^2 + 2n_j} \quad (31)$$

where we have set $\epsilon_{n_j} = s_j(\epsilon - v_j)$ and $s_j = \text{sign}(\epsilon_{n_j} - v_j)$ corresponding to positive and negative energy solutions. The second spinor component now reads as

$$\varphi_j^- = s_j i \sqrt{\frac{\epsilon_{n_j} l_{B_j} - s_j \mu_j l_{B_j}}{\epsilon_{n_j} l_{B_j} + s_j \mu_j l_{B_j}}} |n_j\rangle. \quad (32)$$

After normalization we arrive at the expression for the positive and negative energy eigenstates

$$\psi_j = \frac{1}{\sqrt{2}} \begin{pmatrix} \sqrt{\frac{\epsilon_{n_j} l_{B_j} + s_j \mu_j l_{B_j}}{\epsilon_{n_j} l_{B_j}}} |n_j - 1\rangle \\ s_j i \sqrt{\frac{\epsilon_{n_j} l_{B_j} - s_j \mu_j l_{B_j}}{\epsilon_{n_j} l_{B_j}}} |n_j\rangle \end{pmatrix}. \quad (33)$$

Introducing the parabolic cylinder functions $D_{n_j}(x) = 2^{-\frac{n_j}{2}} e^{-\frac{x^2}{4}} H_{n_j}\left(\frac{x}{\sqrt{2}}\right)$ to express the solution in regions 2, 3 and 4 as

$$\psi_j^\pm(x, y) = \frac{1}{\sqrt{2}} \begin{pmatrix} \sqrt{\frac{\epsilon_{n_j} l_{B_j} + s_j \mu_j l_{B_j}}{\epsilon_{n_j} l_{B_j}}} D\left(\left(\epsilon_{n_j} l_{B_j}\right)^2 - (\mu_j l_{B_j})^2\right)^{1/2-1} \left(\pm\sqrt{2}\left(\frac{x}{l_{B_j}} + k_y l_{B_j}\right)\right) \\ \frac{\pm i s_j \sqrt{2}}{\sqrt{\epsilon_{n_j} l_{B_j} (\epsilon_{n_j} l_{B_j} + s_j \mu_j l_{B_j})}} D\left(\left(\epsilon_{n_j} l_{B_j}\right)^2 - (\mu_j l_{B_j})^2\right)^{1/2} \left(\pm\sqrt{2}\left(\frac{x}{l_{B_j}} + k_y l_{B_j}\right)\right) \end{pmatrix} e^{ik_y y}. \quad (34)$$

In summary the solutions of the energy spectrum in the barrier ($-d_2 \leq x \leq -d_1$) (region 2) are

$$\epsilon_2 = v_2 + s_2 \frac{1}{l_{B_2}} \sqrt{(\mu_2 l_{B_2})^2 + 2n_2} \quad (35)$$

$$\psi_2(x, y) = a_2 \psi_2^+ + b_2 \psi_2^- \quad (36)$$

while in region 3 ($|x| \leq d_1$) read as

$$\epsilon_3 = v_3 + s_3 \frac{1}{l_{B_3}} \sqrt{(\mu_3 l_{B_3})^2 + 2n_3} \quad (37)$$

$$\psi_3(x, y) = a_3 \psi_3^+ + b_3 \psi_3^- \quad (38)$$

and finally in region 4 ($d_1 \leq x \leq d_2$) it can be expressed as

$$\epsilon_4 = v_2 + s_4 \frac{1}{l_{B_2}} \sqrt{(\mu_2 l_{B_2})^2 + 2n_4} \quad (39)$$

$$\psi_4(x, y) = a_4 \psi_4^+ + b_4 \psi_4^- \quad (40)$$

where the parameters a_j and b_j , with $(j = 2, 3, 4)$, are normalization constants.

Recall that, from the above analysis, we ended up with different energy spectra ϵ_2 , ϵ_3 and ϵ_4 , which are obtained in terms of system parameters and quantum numbers in each regions. On the other hand, energy conservation requires that

$$\epsilon = \epsilon_2 = \epsilon_3 = \epsilon_4 \quad (41)$$

and by replacing the energies by their expressions, it is easy to observe that the allowed energy values should satisfy the relation

$$n_2 = n_4 = \frac{l_{B_2}^2}{2} \left[\left(v_3 - v_2 + s_3 \sqrt{\mu_3^2 + \frac{2n_3}{l_{B_3}^2}} \right)^2 - \mu_2^2 \right]. \quad (42)$$

Having obtained all solutions of the energy spectrum, we will see how they can be used to investigate different physical properties of our system. Specifically, we evaluate the transmission and reflection amplitudes in terms of different physical system parameters.

3 Transmission and phase shift

Before determining explicitly the transmission coefficient and its associated phase shift, we notice that total internal reflection will take place only when $0 < \phi_1 < \frac{\pi}{2}$, since the wave incident from the right-hand and left-hand side of the normal surface will behave differently [20]. It is clear that the shift in p_y is due to our choice of gauge for the vector potential. We find it more convenient to parameterize the momenta by

$$p_{x1} = \epsilon \cos \phi_1, \quad p_y = \epsilon \sin \phi_1 + \frac{1}{l_{B_2}^2} (d_2 - d_1) + \frac{d_1}{l_{B_3}^2} \quad (43)$$

$$p_{x5} = \epsilon \cos \phi_5, \quad p_y = \epsilon \sin \phi_5 - \frac{1}{l_{B_2}^2} (d_2 - d_1) - \frac{d_1}{l_{B_3}^2}. \quad (44)$$

It is clear that the refraction angles ϕ_5 at the interfaces are obtained by requiring conservation of the momentum p_y . This leads to a simplified expression of these angles in terms of ϕ_1

$$\sin \phi_5 = \sin \phi_1 + \frac{2}{\epsilon l_{B_2}^2} (d_2 - d_1) + \frac{2d_1}{\epsilon l_{B_3}^2} \quad (45)$$

and therefore we characterize our waves by introducing a critical angle ϕ_c

$$\phi_c = \sin^{-1} \left[1 + 2d_1 \left(\frac{1}{\epsilon l_{B_2}^2} - \frac{1}{\epsilon l_{B_3}^2} \right) - \frac{2d_2}{\epsilon l_{B_2}^2} \right]. \quad (46)$$

This tells us that when the incident angle is less than ϕ_c , the modes become oscillating guided modes, while in the case when the incident angle is more than ϕ_c , we obtain decaying or evanescent wave modes.

In the forthcoming analysis, we will be interested in studying the situation where $\phi_1 < \phi_c$. To simplify our task and proceed further, let us choose the interfaces separating regions as

$$a_{n_j} = \sqrt{\frac{\epsilon_{n_j} l_{B_j} + s_j \mu_j l_{B_j}}{\epsilon_{n_j} l_{B_j}}}, \quad b_{n_j} = \frac{s_j \sqrt{2}}{\sqrt{\epsilon_{n_j} l_{B_j} (\epsilon_{n_j} l_{B_j} + s_j \mu_j l_{B_j})}}. \quad (47)$$

We match the wave functions at the boundaries $(-d_2, -d_1, d_1, d_2)$ as required by the first order nature of the Dirac equation. For this, we introduce the shorthand notations

$$\eta_{1n_2}^\pm = D_{((\epsilon_{n_2} l_{B_2})^2 - (\mu_2 l_{B_2})^2)/2-1} \left(\pm \sqrt{2} \left(\frac{-d_2}{l_{B_2}} + k_y l_{B_2} \right) \right) \quad (48)$$

$$\xi_{1n_2}^\pm = D_{((\epsilon_{n_2} l_{B_2})^2 - (\mu_2 l_{B_2})^2)/2} \left(\pm \sqrt{2} \left(\frac{-d_2}{l_{B_2}} + k_y l_{B_2} \right) \right) \quad (49)$$

the related symbols $\eta_{2n_2}^\pm, \xi_{2n_2}^\pm$ follow by letting $-d_2 \rightarrow -d_1$,

$$\eta_{1n_3}^\pm = D_{((\epsilon_{n_3} l_{B_3})^2 - (\mu_3 l_{B_3})^2)/2-1} \left(\pm \sqrt{2} \left(\frac{-d_1}{l_{B_3}} + k_y l_{B_3} \right) \right) \quad (50)$$

$$\xi_{1n_3}^\pm = D_{((\epsilon_{n_3} l_{B_3})^2 - (\mu_3 l_{B_3})^2)/2} \left(\pm \sqrt{2} \left(\frac{-d_1}{l_{B_3}} + k_y l_{B_3} \right) \right) \quad (51)$$

the related symbols $\eta_{2n_3}^\pm, \xi_{2n_3}^\pm$ follow by letting $-d_1 \rightarrow d_1$,

$$\eta_{1n_4}^\pm = D_{((\epsilon_{n_4} l_{B_2})^2 - (\mu_2 l_{B_2})^2)/2-1} \left(\pm \sqrt{2} \left(\frac{d_1}{l_{B_2}} + k_y l_{B_2} \right) \right) \quad (52)$$

$$\xi_{1n_4}^\pm = D_{((\epsilon_{n_4} l_{B_2})^2 - (\mu_2 l_{B_2})^2)/2} \left(\pm \sqrt{2} \left(\frac{d_1}{l_{B_2}} + k_y l_{B_2} \right) \right) \quad (53)$$

the related symbols $\eta_{2n_4}^\pm, \xi_{2n_4}^\pm$ follow by letting $d_1 \rightarrow d_2$. Now, requiring the continuity of the spinor wavefunctions at each junction interface give rise to a set of equations which can be expressed in terms of 2×2 transfer matrices between different regions

$$\begin{pmatrix} a_j \\ b_j \end{pmatrix} = M_{jj+1} \begin{pmatrix} a_{j+1} \\ b_{j+1} \end{pmatrix} \quad (54)$$

where M_{jj+1} is a transfer matrix that couple the wave function in the j -th region to the wave function in the $(j+1)$ -th region. Finally, we obtain the full transfer matrix over the whole double barrier region, which can be expressed in an obvious notation as

$$\begin{pmatrix} a_1 \\ b_1 \end{pmatrix} = \prod_{j=1}^4 M_{jj+1} \begin{pmatrix} a_5 \\ b_5 \end{pmatrix} = M \begin{pmatrix} a_5 \\ b_5 \end{pmatrix}. \quad (55)$$

The total transfer matrix $M = M_{12} \cdot M_{23} \cdot M_{34} \cdot M_{45}$ is a transfer matrix that couple the wave function in the incident region to the wave function in the transmission region. It can be expressed explicitly as

$$M = \begin{pmatrix} m_{11} & m_{12} \\ m_{21} & m_{22} \end{pmatrix} \quad (56)$$

$$M_{12} = \begin{pmatrix} e^{-ip_x d_2} & e^{ip_x d_2} \\ z_1 e^{-ip_x d_2} & -z_1^* e^{ip_x d_2} \end{pmatrix}^{-1} \begin{pmatrix} a_{n_2} \eta_{1n_2}^+ & a_{n_2} \eta_{1n_2}^- \\ ib_{n_2} \xi_{1n_2}^+ & -ib_{n_2} \xi_{1n_2}^- \end{pmatrix} \quad (57)$$

$$M_{23} = \begin{pmatrix} a_{n_2} \eta_{2n_2}^+ & a_{n_2} \eta_{2n_2}^- \\ ib_{n_2} \xi_{2n_2}^+ & -ib_{n_2} \xi_{2n_2}^- \end{pmatrix}^{-1} \begin{pmatrix} a_{n_3} \eta_{1n_3}^+ & a_{n_3} \eta_{1n_3}^- \\ ib_{n_3} \xi_{1n_3}^+ & -ib_{n_3} \xi_{1n_3}^- \end{pmatrix} \quad (58)$$

$$M_{34} = \begin{pmatrix} a_{n_3} \eta_{2n_3}^+ & a_{n_3} \eta_{2n_3}^- \\ ib_{n_3} \xi_{2n_3}^+ & -ib_{n_3} \xi_{2n_3}^- \end{pmatrix}^{-1} \begin{pmatrix} a_{n_2} \eta_{1n_4}^+ & a_{n_2} \eta_{1n_4}^- \\ ib_{n_2} \xi_{1n_4}^+ & -ib_{n_2} \xi_{1n_4}^- \end{pmatrix} \quad (59)$$

$$M_{45} = \begin{pmatrix} a_{n_2} \eta_{2n_4}^+ & a_{n_2} \eta_{2n_4}^- \\ ib_{n_2} \xi_{2n_4}^+ & -ib_{n_2} \xi_{2n_4}^- \end{pmatrix}^{-1} \begin{pmatrix} e^{ip_x d_2} & e^{-ip_x d_2} \\ z_5 e^{ip_x d_2} & -z_5^* e^{-ip_x d_2} \end{pmatrix}. \quad (60)$$

We consider an electron propagating from left to right with energy ϵl_{B_2} , then $r = b_1$ and $t = a_5$, r and t being the reflection and transmission amplitudes, respectively. We have assumed an incident wave

from left normalized to unit amplitude $a_1 = 1$ and $b_5 = 0$ is the null amplitude due absence of left moving waves in transmission region. This will give rise to the following relations

$$t = \frac{1}{m_{11}}, \quad r = \frac{m_{21}}{m_{11}}. \quad (61)$$

This last formulation will be much more adequate in dealing with periodic systems and applying Bloch theorem to find the associated energy bands. The above expressions can be written as

$$t = \frac{1}{|m_{11}|} e^{i\varphi_t}, \quad r = \left| \frac{m_{21}}{m_{11}} \right| e^{i\varphi_r} \quad (62)$$

where φ_t and φ_r refers to the phase of the transmission and reflection amplitudes, respectively. After a lengthy but straightforward algebra, we can show that t in (62) takes the form

$$t = s_3 a_{n_2}^2 b_{n_2}^2 a_{n_3} b_{n_3} \lambda_{n_2} \lambda_{n_3} \lambda_{n_4} \frac{\Lambda^+ \chi^+ + \Lambda^- \chi^- + i(\Lambda^- \chi^+ - \Lambda^+ \chi^-)}{(\chi^+)^2 + (\chi^-)^2} \quad (63)$$

where we have set

$$\begin{aligned} \Lambda^+ &= (1 + (q_1^+)^2 - (q_1^-)^2) \sin(d_2(p_{x1} + p_{x5})) - 2q_1^+ q_1^- \cos(d_2(p_{x1} + p_{x5})) \\ \Lambda^- &= (1 + (q_1^+)^2 - (q_1^-)^2) \cos(d_2(p_{x1} + p_{x5})) + 2q_1^+ q_1^- \sin(d_2(p_{x1} + p_{x5})) \\ \chi^+ &= -a_{n_2}^2 b_{n_3}^2 \beta_{n_3} D - a_{n_3}^2 b_{n_2}^2 \alpha_{n_3} C + s_2 s_3 a_{n_2} a_{n_3} b_{n_2} b_{n_3} (q_1^+ B_1 + q_5^+ B_2) \\ &\quad - s_3 a_{n_2}^2 a_{n_3} b_{n_2}^2 b_{n_3} A_1 (q_1^+ q_5^- - q_5^+ q_1^-) \\ \chi^- &= -a_{n_2}^2 b_{n_3}^2 \beta_{n_3} E - a_{n_3}^2 b_{n_2}^2 \alpha_{n_3} F + s_2 s_3 a_{n_2} a_{n_3} b_{n_2} b_{n_3} (q_1^- B_1 + q_5^- B_2) \\ &\quad + s_3 a_{n_2}^2 a_{n_3} b_{n_2}^2 b_{n_3} ((q_1^+ q_5^+ - q_1^- q_5^-) A_1 + A_2) \\ A_1 &= \delta_{n_2} \delta_{n_3} \delta_{n_4} + \beta_{n_2} \gamma_{n_3} \alpha_{n_4} \\ A_2 &= \gamma_{n_2} \gamma_{n_3} \gamma_{n_4} + \alpha_{n_2} \delta_{n_3} \beta_{n_4} \\ B_1 &= b_{n_2}^2 (\beta_{n_2} \gamma_{n_3} \gamma_{n_4} + \delta_{n_2} \delta_{n_3} \beta_{n_4}) \\ B_2 &= -a_{n_2}^2 (\alpha_{n_2} \delta_{n_3} \delta_{n_4} + \gamma_{n_2} \gamma_{n_3} \alpha_{n_4}) \\ C &= q_5^+ a_{n_2} \delta_{n_4} (s_2 q_1^- b_{n_2} \beta_{n_2} + a_{n_2} \gamma_{n_2}) + s_2 b_{n_2} q_1^+ \beta_{n_2} (q_5^- a_{n_2} \alpha_{n_4} - s_2 b_{n_2} \gamma_{n_4}) \\ D &= q_5^+ a_{n_2} \alpha_{n_4} (a_{n_2} \alpha_{n_2} - s_2 b_{n_2} \delta_{n_2}) + s_2 q_1^+ b_{n_2} \delta_{n_2} (q_5^- a_{n_2} \alpha_{n_4} - s_2 b_{n_2} \gamma_{n_4}) \\ E &= (a_{n_2} \alpha_{n_2} - s_2 b_{n_2} \delta_{n_2}) (q_5^- a_{n_2} \alpha_{n_4} - s_2 b_{n_2} \gamma_{n_4}) - s_2 q_5^+ a_{n_2} \alpha_{n_4} q_1^+ b_{n_2} \delta_{n_2} \\ F &= (s_2 q_1^- b_{n_2} \beta_{n_2} + a_{n_2} \gamma_{n_2}) (q_5^- a_{n_2} \alpha_{n_4} - s_2 b_{n_2} \gamma_{n_4}) - s_2 q_5^+ a_{n_2} \delta_{n_4} b_{n_2} q_1^+ \beta_{n_2} \\ z_j &= q_j^+ + i q_j^- \\ \alpha_{n_j} &= \eta_{1n_j}^- \eta_{2n_j}^+ - \eta_{1n_j}^+ \eta_{2n_j}^- \\ \beta_{n_j} &= \xi_{1n_j}^- \xi_{2n_j}^+ - \xi_{1n_j}^+ \xi_{2n_j}^- \\ \gamma_{n_j} &= \eta_{1n_j}^- \xi_{2n_j}^+ + \eta_{1n_j}^+ \xi_{2n_j}^- \\ \delta_{n_j} &= \eta_{2n_j}^- \xi_{1n_j}^+ + \eta_{2n_j}^+ \xi_{1n_j}^- \\ \lambda_{n_j} &= \eta_{2n_j}^- \xi_{2n_j}^+ + \eta_{2n_j}^+ \xi_{2n_j}^- \end{aligned}$$

The phase shift can be expressed explicitly as

$$\varphi_t = \arctan \left[\frac{\Lambda^- \chi^+ - \Lambda^+ \chi^-}{\Lambda^+ \chi^+ + \Lambda^- \chi^-} \right] \quad (64)$$

with the quantities

$$\Lambda^- \chi^+ - \Lambda^+ \chi^- = 2 \cos \phi_1 (\chi^+ \cos(\phi_1 + (p_{x1} + p_{x5})) - \chi^- \sin(\phi_1 - (p_{x1} + p_{x5}))) \quad (65)$$

$$\Lambda^+ \chi^+ + \Lambda^- \chi^- = 2 \cos \phi_1 (\chi^+ \sin(\phi_1 - (p_{x1} + p_{x5})) + \chi^- \cos(\phi_1 + (p_{x1} + p_{x5}))). \quad (66)$$

Finally the transmission phase is given by

$$\varphi_t = \tan^{-1} \left[\frac{\chi^+ \cos(\phi_1 + (p_{x1} + p_{x5})) - \chi^- \sin(\phi_1 - (p_{x1} + p_{x5}))}{\chi^+ \sin(\phi_1 - (p_{x1} + p_{x5})) + \chi^- \cos(\phi_1 + (p_{x1} + p_{x5}))} \right]. \quad (67)$$

Now we are ready for the computation of the transmission T and reflection R coefficients. For this purpose, we introduce the associated current density J , which defines T and R as

$$T = \frac{J_{\text{tra}}}{J_{\text{inc}}}, \quad R = \frac{J_{\text{ref}}}{J_{\text{inc}}} \quad (68)$$

where J_{inc} , J_{ref} and J_{tra} stand for the incident, reflected and transmitted components of the current density, respectively. It is easy to show that the current density J reads as

$$J = ev_F \psi^\dagger \sigma_x \psi \quad (69)$$

which gives the following results for the incident, reflected and transmitted components

$$J_{\text{inc}} = ev_F (\psi_1^+)^\dagger \sigma_x \psi_1^+ \quad (70)$$

$$J_{\text{ref}} = ev_F (\psi_1^-)^\dagger \sigma_x \psi_1^- \quad (71)$$

$$J_{\text{tra}} = ev_F (\psi_5^+)^\dagger \sigma_x \psi_5^+. \quad (72)$$

The energy conservation

$$\left[p_{x1}^2 + (p_y + \frac{1}{l_{B2}^2} (d_1 - d_2) - \frac{1}{l_{B3}^2} d_1)^2 \right]^{\frac{1}{2}} = \left[p_{x5}^2 + (p_y + \frac{1}{l_{B2}^2} (d_2 - d_1) + \frac{1}{l_{B3}^2} d_1)^2 \right]^{\frac{1}{2}} \quad (73)$$

allows us to express the transmission and reflection probabilities in the following simple forms

$$T = \frac{p_{x5}}{p_{x1}} \frac{1}{|m_{11}|^2}, \quad R = \left| \frac{m_{21}}{m_{11}} \right|^2. \quad (74)$$

More explicitly the transmission coefficient T reads as

$$T = \frac{4p_{x5} (\cos \phi_1)^2}{p_{x1} [(\chi^+)^2 + (\chi^-)^2]} a_{n2}^4 b_{n2}^4 a_{n3}^2 b_{n3}^2 \lambda_{n2}^2 \lambda_{n3}^2 \lambda_{n4}^2. \quad (75)$$

Obviously, R and T are not independent, they are related through the unitarity requirement $T + R = 1$ that is clearly shown in Figure 2a. Note that (45) implies that for certain incidence angles ϕ_1 the transmission is not allowed. In fact for

$$\epsilon l_{B2} \leq \frac{1}{l_{B2}} (d_2 - d_1) + \frac{d_1}{l_{B2}} \left(\frac{l_{B2}}{l_{B3}} \right)^2 \quad (76)$$

all waves are completely reflected.

We show the numerical results for the transmission, reflection coefficients and the GHl shifts in Figures 2, 3, 4, 5, 6, for several parameter values (ϵ , v_2 , v_3 , μ_j , d_1 , d_2). For instance a typical value

of the magnetic field, say $B_2 = 4T$, the magnetic length is $l_{B_2} = 13nm$, and $\epsilon l_{B_2} = 1$ corresponding to the energy $E = 44meV$ [7], these typical values will serve to normalize the various variables. The polar graph, Figure 2b, shows the transmission as a function of the incidence angle, the outermost circle corresponds to full transmission, $T = 1$, while the origin of this plot represents zero transmission. Requiring that $\epsilon l_{B_2} = 3.7$, $d_2 = d_1$, $l_{B_2} = l_{B_3}$, $v_2 = v_3 = 0$, $\frac{d_1}{l_{B_2}} = \{0.5, 1.5, 3, 3.67\}$ and $\mu_j = 0$ reproduces exactly the result obtained in previous work [7]. Similarly, the transmission as a function of energy ϵ for fixed $\frac{d_2}{l_{B_2}} = 0.8$, $\frac{d_1}{l_{B_2}} = 0.2$ and $\frac{l_{B_3}}{l_{B_2}} = 0.6$, i.e. $\frac{d_2 - d_1}{l_{B_2}} + \frac{d_1}{l_{B_2}} \left(\frac{l_{B_2}}{l_{B_3}}\right)^2 = 1.156$, shows that the transmission vanishes for $\epsilon l_{B_2} \leq 1.156$.

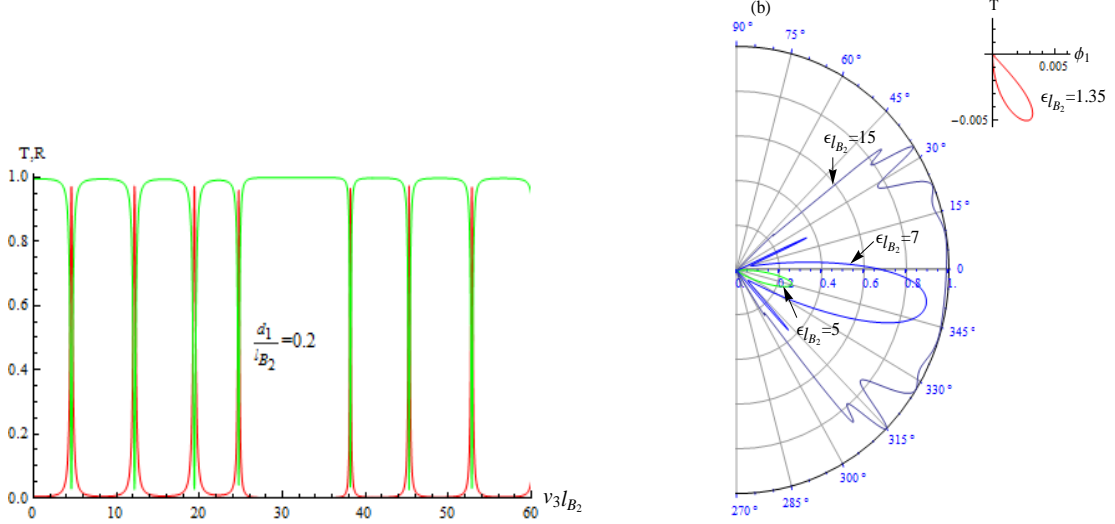


Figure 2: (a): Graphs depicting the reflection R (green line) and transmission T (red line) coefficients as function of energy potential $v_3 l_{B_3}$ for the monolayer graphene barriers with $\frac{d_1}{l_{B_2}} = 0.2$, $\frac{d_2}{l_{B_2}} = 0.8$, $v_2 l_{B_2} = 26$, $\epsilon l_{B_2} = 30$, $k_y l_{B_2} = 1$, $\frac{l_{B_3}}{l_{B_2}} = 2$ and $\mu l_{B_2} = 4$. (b): Polar plot of a curve with radius (transmission T) as a function of angle ϕ_1 with $\epsilon l_{B_2} = \{15, 7, 5, 1.35\}$, $\frac{d_1}{l_{B_2}} = 0.2$, $\frac{d_2}{l_{B_2}} = 0.8$, $\frac{l_{B_3}}{l_{B_2}} = 0.6$, $v_2 l_{B_2} = 3.1$, $v_3 l_{B_2} = 1.2$ and $\mu l_{B_2} = 2$.

4 GHl shifts for double barriers

In this section, we shall turn to the Goos-Hänchen like (GHL) shifts in graphene by considering an incident, reflected and transmitted beams around a given transverse wave vector $k_y = k_{y0}$ and angle of incidence $\phi_1(k_{y0}) \in [0, \frac{\pi}{2}]$, denoted by the subscript 0. These can be expressed in integral form

$$\Psi_i(x, y) = \int_{-\infty}^{+\infty} dk_y f(k_y - k_{y0}) e^{i(k_{x1}(k_y)x + k_y y)} \begin{pmatrix} 1 \\ e^{i\phi_1(k_y)} \end{pmatrix} \quad (77)$$

$$\Psi_r(x, y) = \int_{-\infty}^{+\infty} dk_y r(k_y) f(k_y - k_{y0}) e^{i(-k_{x1}(k_y)x + k_y y)} \begin{pmatrix} 1 \\ -e^{-i\phi_1(k_y)} \end{pmatrix}. \quad (78)$$

The reflection amplitude can be written as $r(k_y) = |r|e^{i\varphi_r}$ because of the x -component of wavevector k_{x1} as well as ϕ_1 are function of k_y , where each spinor plane wave is a solution of (4). The angular

spectral distribution $f(k_y - k_{y0})$ can be assumed of Gaussian shape

$$f(k_y - k_{y0}) = w_y e^{-w_y^2 (k_y - k_{y0})^2} \quad (79)$$

where w_y being the half beam width at waist [18]. We can approximate the k_y -dependent terms by a Taylor expansion around k_{y0} and retain only the first order term to obtain

$$\phi_1(k_y) \approx \phi_1(k_{y0}) + \left. \frac{\partial \phi_1}{\partial k_y} \right|_{k_{y0}} (k_y - k_{y0}) \quad (80)$$

$$k_{x1}(k_y) \approx k_{x1}(k_{y0}) + \left. \frac{\partial k_{x1}}{\partial k_y} \right|_{k_{y0}} (k_y - k_{y0}). \quad (81)$$

The transmitted wave takes the form

$$\Psi_t(x, y) = \int_{-\infty}^{+\infty} dk_y t(k_y) f(k_y - k_{y0}) e^{i(k_{x5}(k_y)x + k_y y)} \begin{pmatrix} 1 \\ e^{i\phi_5(k_y)} \end{pmatrix} \quad (82)$$

where the transmission amplitude $t(k_y) = |t|e^{i\varphi_t}$ is calculated through the use of boundary conditions. In order to determine the GHL shifts of the transmitted beam through the graphene double barriers, we adopt the following definition [21, 22]

$$S_t = - \left. \frac{\partial \varphi_t}{\partial k_y} \right|_{k_{y0}}. \quad (83)$$

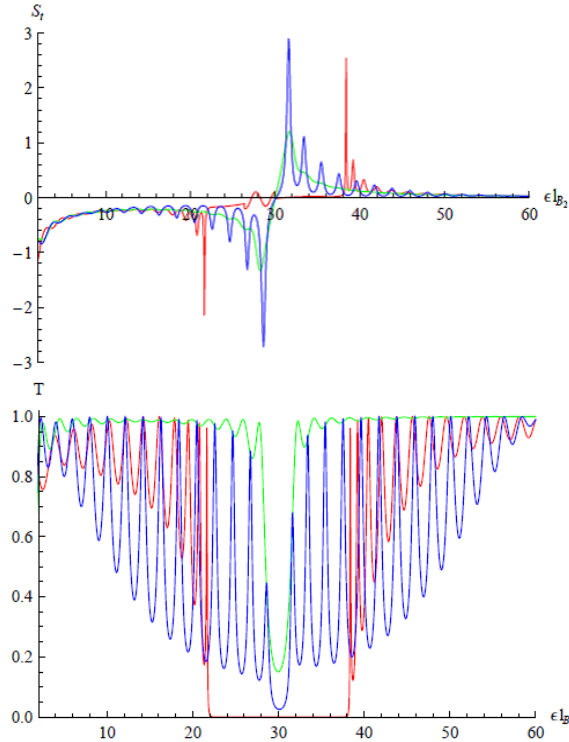


Figure 3: The GHL shifts and the transmission as function of energy ϵl_{B_2} for the monolayer graphene barriers with $\frac{d_2}{l_{B_2}} = 0.8$, $v_2 l_{B_2} = 30$, $v_3 l_{B_2} = 30$, $k_y l_{B_2} = 1$, $\frac{l_{B_2}}{l_{B_3}} = 0.5$, $\frac{d_1}{l_{B_2}} = 0.7$ where $(\mu_2 l_{B_2} = 0, \mu_3 l_{B_2} = 8)$ color red, $(\mu_2 l_{B_2} = 0, \mu_3 l_{B_2} = 0)$ color green and $(\mu_2 l_{B_2} = 8, \mu_3 l_{B_2} = 0)$ color blue.

In Figure 3, the above transmission and GHL shifts are shown versus energy ϵl_{B_2} for different parameters of our system ($\frac{d_2}{l_{B_2}} = 0.8, v_2 l_{B_2} = 30, v_3 l_{B_2} = 30, k_y l_{B_2} = 1, \frac{l_{B_3}}{l_{B_2}} = 2, \frac{d_1}{l_{B_2}} = 0.7$) with zero-gap ($\mu_2 l_{B_2} = \mu_3 l_{B_2} = 0$): green color and finite gap ($\mu_2 l_{B_2} = 0, \mu_3 l_{B_2} = 8$): red color and ($\mu_2 l_{B_2} = 8, \mu_3 l_{B_2} = 0$): blue color. It is clearly seen that GHL shifts are oscillating between negative and positive values around the critical point $\epsilon l_B = v_2 l_B = v_3 l_B$. The quantity $k_y l_B = m^*$ plays a very important role in the transmission of Dirac fermions via obstacles created by a series of scattering potentials, because it is associated with the effective mass of the particle and hence determines the threshold for allowed energies. However, in the presence of an inhomogeneous magnetic field in the regions $|x| \leq d_2$, it reduces this effective mass to $\left(p_y + \frac{1}{l_{B_2}^2} (d_1 - d_2) - \frac{d_1}{l_{B_3}^2}\right)$ in the incidence region while it increases it to $\left(p_y - \frac{1}{l_{B_2}^2} (d_1 - d_2) + \frac{d_1}{l_{B_3}^2}\right)$ in the transmission region. The allowed energies are then determined by the greater effective mass condition:

$$\epsilon l_{B_2} \geq p_y - \frac{1}{l_{B_2}^2} (d_1 - d_2) + \frac{d_1}{l_{B_3}^2}$$

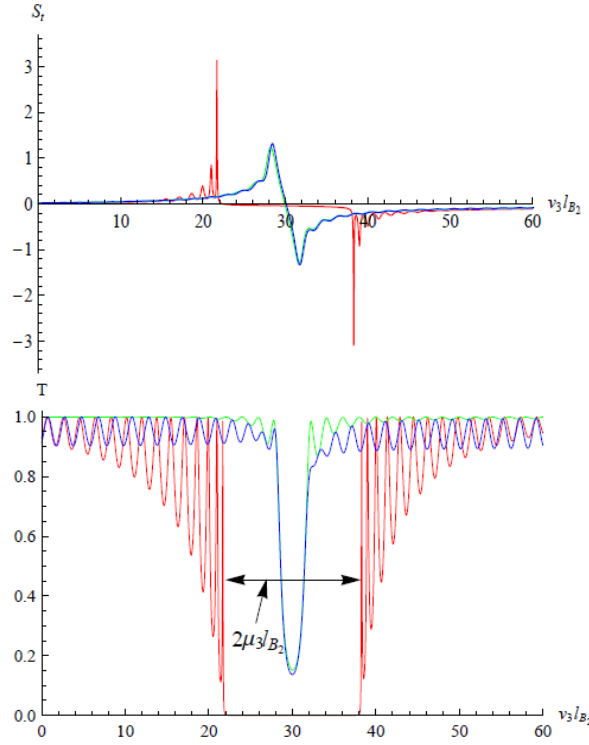


Figure 4: The GHL shifts and the transmission as function of the potential $v_3 l_{B_2}$ for the monolayer graphene barriers with $\frac{d_2}{l_{B_2}} = 0.8, v_2 l_{B_2} = 27, \epsilon l_{B_2} = 30, k_y l_{B_2} = 1, \frac{l_{B_3}}{l_{B_2}} = 2, \frac{d_1}{l_{B_2}} = 0.78$ where ($\mu_2 l_{B_2} = 0, \mu_3 l_{B_2} = 8$) color red, ($\mu_2 l_{B_2} = 0, \mu_3 l_{B_2} = 0$) color green and ($\mu_2 l_{B_2} = 8, \mu_3 l_{B_2} = 0$) color blue.

The above GHL shifts and transmission are plotted in Figure 4 in terms of the potential $v_3 l_{B_2}$ for some values of the physical parameters. It is clearly seen that S_t is oscillating between negative and

positive values around the critical point $v_3 l_{B_2} = \epsilon l_{B_2}$. At such points the transmission vanishes for $\epsilon l_{B_2} - \mu_3 l_{B_2} \leq v_3 l_{B_2} \leq \epsilon l_{B_2} + \mu_3 l_{B_2}$ and oscillates otherwise.

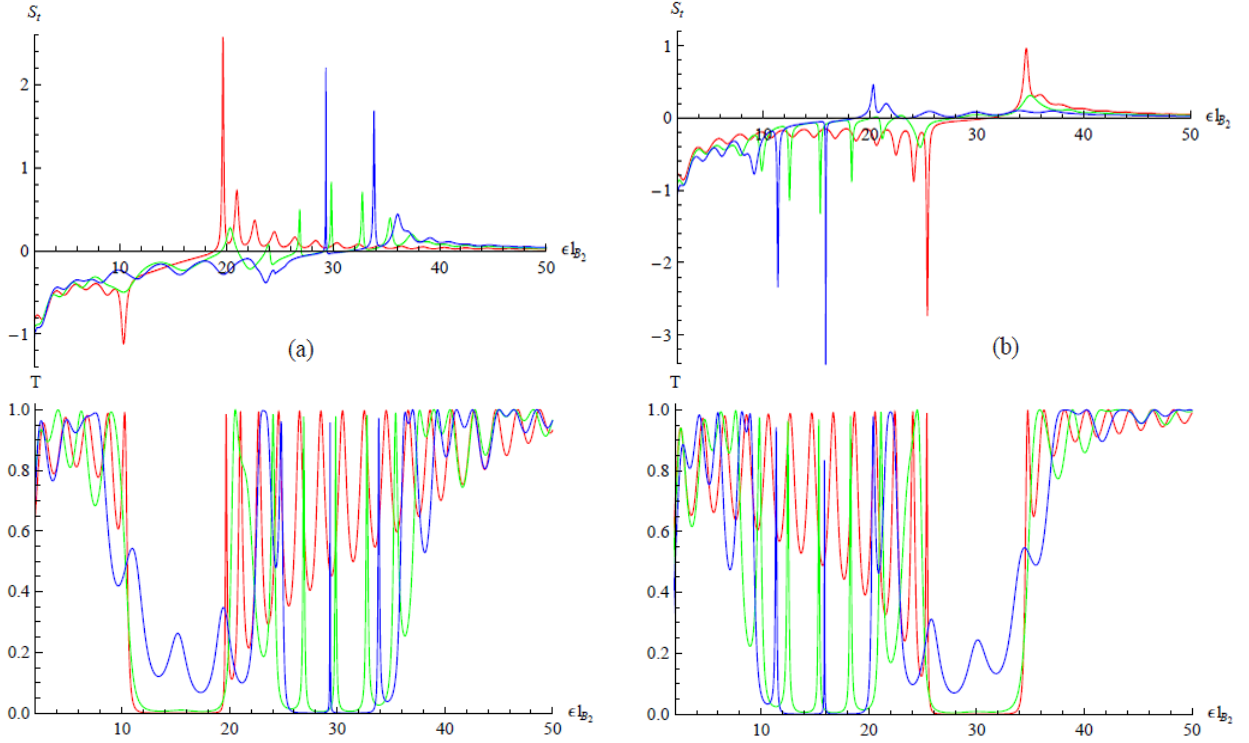


Figure 5: The GHL shifts and the transmission as function of energy ϵl_{B_2} for the monolayer graphene barriers. (a)/(b) with $(v_2 l_{B_2} = 30, v_3 l_{B_2} = 15)/(v_2 l_{B_2} = 15, v_3 l_{B_2} = 30)$, with $\frac{d_2}{l_{B_2}} = 0.8$, $k_y l_{B_2} = 1$, $\frac{l_{B_3}}{l_{B_2}} = 2$, $\mu_2 l_{B_2} = \mu_3 l_{B_2} = 4$, $\frac{d_1}{l_{B_2}} = 0.19$ (blue line), $\frac{d_1}{l_{B_2}} = 0.4$ (green line) and $\frac{d_1}{l_{B_2}} = 0.7$ (red line).

In Figure 5, the transmission and GHL shifts are shown versus energy ϵl_{B_2} . One can notice that at the Dirac points ($\epsilon l_{B_2} = v_2 l_{B_2}$, $\epsilon l_{B_2} = v_3 l_{B_2}$), the GHL shifts change their sign. This change shows clearly that they are strongly dependent on the barrier heights. We also observe that the GHL shifts are positive as long as the energy satisfies the condition $\epsilon l_{B_2} > v_2 l_{B_2} > v_3 l_{B_2}$ (Figure 5a) and negative for $\epsilon l_{B_2} < v_2 l_{B_2} < v_3 l_{B_2}$ (Figure 5b.)

In Figure 6, we analyze the transmission coefficients versus the potential $v_3 l_{B_2}$ and $v_2 l_{B_2}$. In doing so, we fix the energy $\epsilon l_{B_2} = 30$ and choose a value of $\frac{d_1}{l_{B_2}}$, then we compute the transmission as shown in Figure 6a. We notice that the transmission decreases if $\frac{d_1}{l_{B_2}}$ increases and then vanishes while Figure 6b shows different behavior. Note that, the Dirac points represent the zero modes for Dirac operator [16] and lead to the emergence of new Dirac points, which has been discussed in different works [23,24]. Such points separate the two regions of positive and negative refraction. In cases where $v_2 l_{B_2} < \epsilon l_{B_2}$ and $v_2 l_{B_2} > \epsilon l_{B_2}$ (respectively $v_3 l_{B_2} < \epsilon l_{B_2}$ and $v_2 l_{B_2} > \epsilon l_{B_2}$), the shifts are respectively in the forward and backward directions, due to the fact that the signs of the group velocity are opposite.

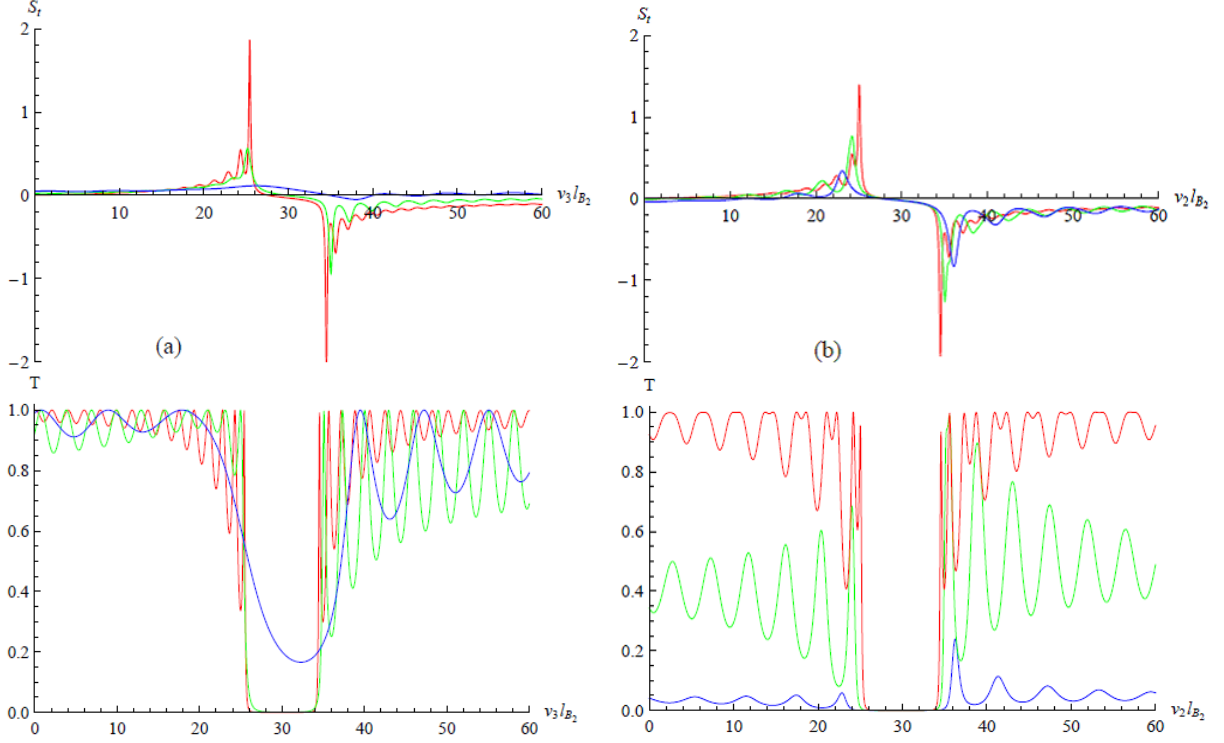


Figure 6: The GHL shifts and the transmission as function of energy potential $v_3 l_{B_2}$ and $v_2 l_{B_2}$ for the monolayer graphene barriers. (a): $\epsilon l_{B_2} = 30$, $v_2 l_{B_2} = 15$, $\frac{d_2}{l_{B_2}} = 0.8$, $k_y l_{B_2} = 1$, $\frac{l_{B_3}}{l_{B_2}} = 2$, $\mu_2 l_{B_2} = \mu_3 l_{B_2} = 4$, $\frac{d_1}{l_{B_2}} = 0.2$ (blue line), $\frac{d_1}{l_{B_2}} = 0.5$ (green line) and $\frac{d_1}{l_{B_2}} = 0.78$ (red line). (b): $\epsilon l_{B_2} = 30$, $v_3 l_{B_2} = 32$, $\frac{d_2}{l_{B_2}} = 0.8$, $k_y l_{B_2} = 1$, $\frac{l_{B_3}}{l_{B_2}} = 2$, $\mu l_{B_2} = 4$, $\frac{d_1}{l_{B_2}} = 0.3$ (blue line), $\frac{d_1}{l_{B_2}} = 0.12$ (green line) and $\frac{d_1}{l_{B_2}} = 0.02$ (red line).

5 Conclusion

To conclude, we have studied the transport of electrons in graphene scattered by double barrier in the presence of an inhomogeneous magnetic field. We obtained the solutions for the energy spectrum taking into account the conservation energy and noticed that for certain incidence angles the transmission is not allowed for $\epsilon l_{B_2} \leq p_y - \frac{1}{l_{B_2}^2}(d_1 - d_2) + \frac{1}{l_{B_3}^2}d_1$. However, the transmission probability T does not vanish in general, we also found that, in contrast to electrostatic barriers, magnetic barriers are able to confine Dirac fermions. This allowed us to calculate the GHL shifts of reflected and transmitted electron beams in a graphene double barrier structure in the presence of an inhomogeneous magnetic field. We also established some correlation between the electronic transport properties of Dirac fermions with the GHL shifts.

The numerical data showed how these shifts behave in relation to the transmission probability T . It is found that the GHL shifts can be modulated by the incident energy ϵl_{B_2} , potential energies $v_2 l_{B_2}$ and $v_3 l_{B_2}$. The GHL shifts still change sign, but the point where it changes sign has been displaced to the left and the absolute value of the maximum of the shifts increased as well. Thus we seen that the GHL shifts in the transmission region can be either negative or positive.

Acknowledgments

The generous support provided by the Saudi Center for Theoretical Physics (SCTP) is highly appreciated by all authors. H.B. Also acknowledges the support of King Fahd University of Petroleum and Minerals to the Theoretical Physics Research Group.

References

- [1] K. S. Novoselov, A. K. Geim, S. V. Morozov, D. Jiang, M. I. Katsnelson, I. V. Grigorieva, S. V. Dubonos and A. A. Firsov, *Nature* 438, 197 (2005).
- [2] R. Nair, P. Blake, A. Grigorenko, K. Novoselov, T. Booth, T. Stauber, N. Peres and A. Geim, *Science* 320, 1308 (2008).
- [3] M. I. Katsnelson, K. S. Novoselov and A. K. Geim, *Nature Phys.* 2, 620 (2006).
- [4] A. F. Young and P. Kim, *Nature Phys.* 5, 222 (2009).
- [5] K. S. Novoselov, A. K. Geim, S. V. Morozov, D. Jiang, Y. Zhang, S. V. Dubonos, I. V. Grigorieva and A. A. Firsov, *Science* 306, 666 (2004).
- [6] Yuanbo Zhang, Yan-Wen Tan, H. L. Störmer and P. Kim, *Nature* 438, 201 (2005).
- [7] A. De Martino, L. Dell'Anna and R. Egger, *Phys. Rev. Lett.* 98, 066802 (2007).
- [8] P. D. Ye, D. Weiss, R. R. Gerhardts, M. Seeger, K. von Klitzing, K. Eberl and H. Nickel, *Phys. Rev. Lett.* 74, 3013 (1995).
- [9] D. Lawton, A. Nogaret, M. V. Makarenko, O. V. Kibis, S. J. Bending and M. Henini, *Physica E* 13, 699 (2002).
- [10] T. K. Ghosh, A. De Martino, W. Häusler, L. Dell'Anna and R. Egger, *Phys. Rev. B* 77, 081404(R) (2008).
- [11] X. Chen, J.-W. Tao and Y. Ban, *Eur. Phys. J. B* 79, 203 (2011).
- [12] Y. Song, H-C. Wu and Y. Guo, *Appl. Phys. Lett.* 100, 253116 (2012).
- [13] A. Jellal, I. Redouani, Y. Zahidi and H. Bahlouli, *Physica E* 58, 30 (2014).
- [14] A. Jellal, Y. Wang, Y. Zahidi and M. Miloud, *Physica E* 68, 53 (2015).
- [15] X. Chen, P-L. Zhao, X-J. Lu and L-G. Wang, *Eur. Phys. J. B* 86, 223 (2013).
- [16] M. Sharma and S. J. Ghosh, *J. Phys.: Cond. Matt* 23, 055501 (2011).
- [17] J.-H. Huang, Z.-L. Duan, H.-Y. Ling and W.-P. Zhang, *Phys. Rev. A* 77, 063608 (2008).
- [18] C. W. J. Beenakker, R. A. Sepkhanov, A. R. Akhmerov and J. Tworzydło, *Phys. Rev. Lett.* 102, 146804 (2009).

- [19] L. Zhao and S. F. Yelin, *Phys. Rev. B* 81, 115441 (2010).
- [20] S. Ghosh and M. Sharma, *J. Phys.: Cond. Matt.* 21, 292204 (2009).
- [21] X. Chen, Y. Ban and C.-F. Li, *J. Appl. Phys.* 105, 093710 (2009).
- [22] X. Chen, C.-F. Li and Y. Ban, *Phys. Rev. B* 77, 073307 (2008).
- [23] S. Bhattacharjee, M. Maiti and K. Sengupta, *Phys. Rev. B* 76, 184514 (2007).
- [24] C. H. Park, Y. W. Soon, L. Yang, M. L. Cohen and S. G. Louie, *Phys. Rev. Lett.* 103, 046808 (2009).